Romanian Reports in Physics **71**, 603 (2019)

GLUCOSE DETECTION USING BSA:PEDOT-PSS AS BIOACTIVE SOLUTE AND SOLID BIOACTIVE LAYER DEPOSITED BY SPIN COATING

O. BRÎNCOVEANU[1,2], A. IOANID[1], R. MEȘTERCA[2], A. PANTAZI[1,2], C. MOISE [2], M. ENACHESCU [2,3], S. IFTIMIE, S. ANTOHE [1,3,*]

[1] Faculty of Physics, University of Bucharest, 077125, Romania
[2] Center for Surface Science and Nanotechnology, University Politehnica of Bucharest, 060042 Romania
E-mail: *oana_brincoveanu@yahoo.com*
[3] Academy of Romanian Scientists, Bucharest, 050094, Romania

Received June 8, 2017

Abstract. The two glucose-protein-polymer composite solutions, Glucose: BSA:PEDOT-PSS [10:1:1] and Glucose/BSA:PEDOT-PSS [1:1], were prepared by mixing protein (BSA), polymer (PEDOT-PSS) and glucose solutions for the first sample and protein-polymer-composite (BSA:PEDOT-PSS [1:1]) and glucose solutions for the second sample with both pH and concentration in biological range values. An analysis of the UV-Vis spectrum of the Glucose/BSA:PEDOT-PSS [1:1] solution to determine the glucose concentration and a comparative study using UV-Vis and ATR/FTIR absorption spectra recorded at room temperature for BSA, PEDOT-PSS, BSA:PEDOT-PSS [1:1] and Glucose:BSA:PEDOT-PSS[10:1:1] were performed. Afterwards, both the Glucose: BSA:PEDOT-PSS [10:1:1] and Glucose/BSA:PEDOT-PSS [1:1] solutions were deposited as solid bioactive layer on silicon (100) coated with a silver thin layer by PLD technique. AFM (topography profiles, electrostatic images, $F-z$ curves) and ATR/FTIR techniques were used to identify morphological and compositional characteristics of the solid bioactive layers surface.

Key words: glucose, bioactive layer, Adhesion force, biosensors, bio detection efficiency.

1. INTRODUCTION

The intake of glucose in living organisms constitutes a basic need, because it plays an important role in a wide range of biological processes. In the human body, the blood glucose concentration is well defined in the range $(80 \div 120)$ mg dl^{-1} (respectively $(4.4 \div 6.6)$ mM). In reality, blood glucose concentration measured is within a much larger range $(2 \div 30)$ mM [1, 2]. Diabetes is a disease affecting 5% of the world population and is characterized by a series of metabolic disorders caused by insulin deficiency and hyperglycemia. The disease itself, and the associated health problems, like heart disease, kidney failure and blindness are one of the leading causes of death worldwide. The problem associated with diabetes

can be significantly attenuated through tight control of blood glucose concentration. Therefore, the diagnosis and management of diabetic conditions require close monitoring of the blood glucose concentration. Millions of people are testing glucose levels daily, and about six billion glucose tests are performed each year. Biosensors used for the detection of glucose represents approximately 85% of the entire market of biosensors worldwide [1, 3, 4].

Biosensors represent a new trend developing in terms of theoretical and technological achievements for the design and use of analytical tools in order to detect, quantify and monitor chemical species specific for clinical, environmental or industrial analyses [5]. For this purpose, the protein-polymer composite BSA:PEDOT-PSS [1:1] was used as solid bioactive layer with efficient detection function in a future biosensor design. The use of the composite aims to optimize the bio detection efficiency *via* specific interactions of the layer interfaces with both the analyzed bioactive fluid and its support substrate.

2. MATERIALS AND CHARACTERIZATION TECHNIQUES

Primary substances: Glucose, BSA and PEDOT-PSS were purchased from Sigma-Aldrich Company. BSA solution was prepared with ultrapure and deionized water, using lyophilized powder with ~ 66k Da, pH = 7.0, 2 mM, purity ≥ 95% (agarose gel electrophoresis). The polymer solution was obtained from the emulsion of PEDOT-PSS with the concentration of 1.3 wt.% (PEDOT content 0.5 wt.%; PSS content 0,8 wt.%), 2 mM, 1 S/cm.

The UV-Vis absorption measurements were carried out at room temperature on solution samples with a wide range of concentrations, using spectrometer UV/ VIS/IR-960 from Perkin Elmer. The Glucose:BSA:PEDOT-PSS solutions were prepared by mixing a 2×10^{-4} M BSA:PEDOT-PSS [1:1] solution and glucose solutions with concentrations of 0.01 M, 5×10^{-3} M, 2.5×10^{-3} M, 1.3×10^{-3} M, 6.25×10^{-4} M, 3.13×10^{-4} M, 1.56×10^{-4} M, 7.81×10^{-5} M, 3.91×10^{-5} M, 1.95×10^{-5} M, respectively. The IR absorption measurements, by means of ATR/FTIR technique, were carried out in air atmosphere using Spectrum Two IR spectrometer from Perkin Elmer. The AFM, EFM measurements and F–z curves for the exposed surface of Glucose/ Ag/Si, Glucose:BSA:PEDOT-PSS[10:1:1]/Ag/Si and Glucose/BSA:PEDOT-PSS[1:1]/ Ag/Si structures were compared with those of Ag/Si, BSA/Ag/Si, PEDOT-PSS/Ag/Si and BSA:PEDOT-PSS[1:1]/Ag/Si structures [6]. The AFM and EFM measurements were performend in non-contact mode using a silicon/Pt-coated cantilever with the spring constant of 17 N/m and resonance frequency of 230 kHz, while the $F - z$ curves were performend in contact mode using a silicon cantilever with the spring constant of 0.26 N/m and resonance frequency of 19 kHz. All the measurements were performed with the help of Solver Next (NT-MDT) AFM equipment.

3. RESULTS AND DISCUSSIONS

3.1. UV-VIS SPECTROSCOPY RESULTS

It is known that the UV-Vis absorption spectra which can be utilized to test electrons ensemble properties, constitute a reliable and efficient method used to investigate the molecular structure evolution. In Figure 1a are shown the absorption spectra recorded for Glucose/BSA:PEDOT-PSS[1:1] solution samples having glucose concentration in the (0.00 ÷ 0.02) M range and in the (240 – 320) nm spectral range, while Figure 1b illustrates the dependence of the monochromatic absorbance at λ = 278 nm on glucose concentration. It is observed that the absorption peak at λ = 278 nm, specific both to the BSA and BSA:PEDOT-PSS[1:1] solution, is conserved and its intensity increases with the increasing of glucose concentration. This behavior may be associated with an appreciable increase in the intensity of the HOMO – LUMO dipole type transitions, as $\pi - \pi^*$ orbital molecular transitions.

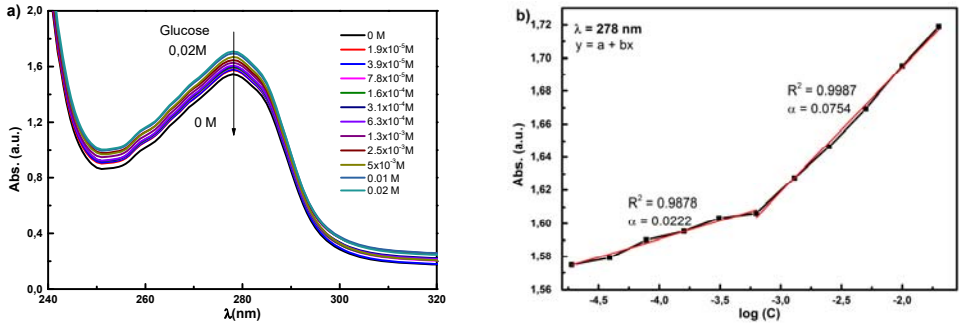

Fig. 1 – Dependence of UV-Vis spectra of solution concentrations: a) absorption spectrum of BSA:PEDOT-PSS[1:1] 2×10^{-4} M composite mixed with different concentrations (0.02 M, 0.01 M, 5×10^{-3} M, 2.5×10^{-3} M, 1.3×10^{-3} M, 6.25×10^{-4} M, 3.13×10^{-4} M, 1.56×10^{-4} M, 7.81×10^{-5} M, 3.91×10^{-5} M, 1.95×10^{-5} M, 0M) of glucose solutions; b) threshold of glucose detection by λ = 278 nm optical absorbance.

The increase of the monochromatic absorbance with the increasing of glucose concentration, indicates the presence of glucose molecules aggregated/bonded to the BSA:PEDOT-PSS[1:1] composite molecules and theirs orbitals overlap, which leads to changes in the π orbital molecular system states between which dipole transitions are induced [1, 7].

According to Beer-Lambert relationship, in the case of a homogeneous solution, the absorbance peak characteristic for the BSA:PEDOT-PSS[1:1] composite solution increases linearly with the concentration of glucose.

The dependence of the absorption intensity at λ = 278 nm on the glucose concentrations from Fig. 1b shows that the Beer-Lambert linear dependence is verified, but on two distinct ranges of glucose concentrations. Thus, for glucose concentrations values higher than 6.25×10^{-4} M, the slope dependence is much higher

(over three times) than for those less than 6.25×10^{-4} M, so that this value can be considered as a threshold value for glucose concentration detection in a test solution.

3.2. FTIR SPECTROSCOPY RESULTS

The molecular structure of the bioactive composite and its development by exposure to the investigated medium, was performed by ATR/FTIR technique, which can provide quantitative information on the evolution of biomolecule secondary structure, and therefore on the target molecules with which it interacts. Thus, ATR/FTIR spectrum was used to characterize the BSA:PEDOT-PSS[1:1] composite with the glucose addition particularities, both as bioactive component solution and as a bioactive layer deposited on a support. In case of the bioactive layer, we analyzed both layers obtained by depositing a solution containing glucose, in two processes: from the Glucose:BSA:PEDOT-PSS[10:1:1] solution obtained by the initial mixture of all components and from the glucose solution deposited on the BSA:PEDOT-PSS[1:1] composite solid layer to obtain Glucose/BSA:PEDOT-PSS[10:1:1]/Ag/Si structure.

For a comparative analysis, in Fig. 2 are shown the ATR/FTIR spectra for independent BSA, PEDOT-PSS, glucose, BSA:PEDOT-PSS[1:1] and Glucose:BSA:PEDOT-PSS[1:1] solutions. All spectra were recorded within the (450 ÷ 4000) cm^{-1} energy range at room temperature. It is known that the common (3000 ÷ 3700) cm^{-1} large absorption band is due to water as solvent, so that to allow comparison, the ordinate shows the values of the rescaled, but ordered to comply with the individual absolute values ratio in (450 ÷ 2000) cm^{-1} energy range.

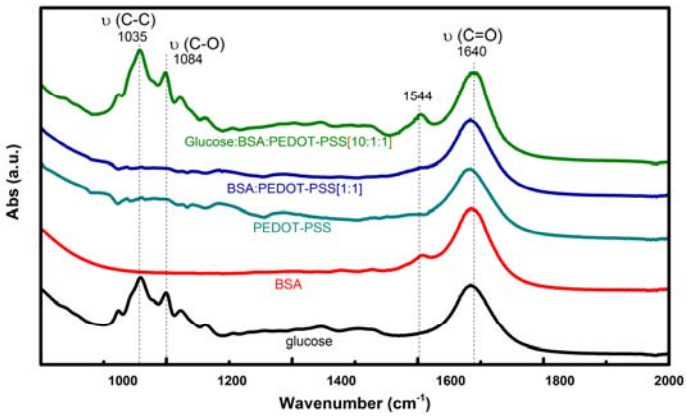

Fig. 2 – FTIR/ATR spectra of Glucose (black), BSA (red), PEDOT-PSS (turquoise), BSA:PEDOT-PSS[1:1] (blue) and Glucose:BSA:PEDOT-PSS[10:1:1] (green) solutions.

A comparative analysis of FTIR/ATR spectra from Fig. 2 reveals that the Glucose:BSA:PEDOT-PSS[10:1:1] solution spectrum cumulates the peaks from

those of the glucose, BSA and PEDOT-PSS solution spectra, suggesting a new molecular structure organization. Thus, the 1.640 cm^{-1} peak assigned to the C = O vibration mode is common to all components. Particulary, the 1.544 cm^{-1} peak is assigned to the Amide II band [8], resulting from N – H bending and C – N stretching vibrations in the protein molecule, the peaks from (1000 ÷ 2000) cm^{-1} range are associated with the C – C and C – O vibration modes from the glucose molecule structure, as well as the C = O vibration mode between the adjacent rings of PEDOT chains structure. The glucose binding to the BSA:PEDOT-PSS[1:1] active solute is evidenced by the presence of absorption peaks associated to the C = O (1640 cm^{-1}), C – O (1084 cm^{-1}) and C – C (1035 cm^{-1}) functional group modes of the glucose molecule structure [9, 10].

In Fig. 3 are presented the comparative ATR/FTIR spectra recorded in the same condition as before, for exposed solid active layer of Glucose/Ag/Si, BSA/Ag/Si, PEDOT-PSS/Ag/Si, BSA:PEDOT-PSS[1:1]/Ag/Si, Glucose:BSA:PEDOT-PSS[10:1:1]/Ag/Si and Glucose/BSA:PEDOT-PSS[1:1]/Ag/Si structures. Both the Glucose:BSA:PEDOT-PSS[10:1:1]/Ag/Si and Glucose/BSA:PEDOT-PSS[1:1]/Ag/Si spectra show peaks specific to both the BSA (~1640 cm^{-1}) and glucose (~1084 cm^{-1}) molecules, but their intensity is more pronounced for Glucose/BSA:PEDOT-PSS[1:1]/Ag/Si layer surface.

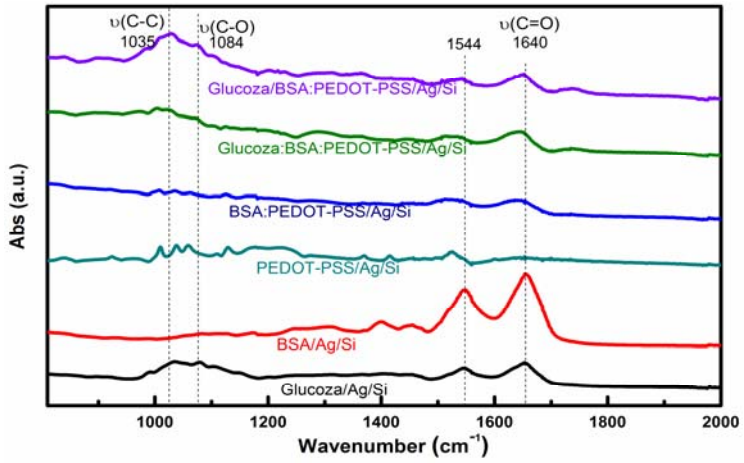

Fig. 3 – ATR/FTIR spectra of Glucose/Ag/Si (black), BSA/Ag/Si (red), PEDOT-PSS/Ag/Si (turquoise), BSA:PEDOT-PSS[1:1]/Ag/Si (blue), Glucose:BSA:PEDOT-PSS[10:1:1]/Ag/Si (green) and Glucose/BSA:PEDOT-PSS[10:1:1]/Ag/Si (mauve) thin films (Color online).

According to the model proposed in [6], while the structural unit of BSA:PEDOT-PSS[1:1] composite in solution is nearly spherical and resulting from the PEDOT chains adhesion to the BSA molecule, mainly *via* dipole – dipole interactions between PEDOT rings and BSA α-helix and β-sheets secondary structures, the BSA:PEDOT-PSS[1:1] active layer is nanostructured, composed of ellipsoidal

nanoparticles consisting of BSA:PEDOT-PSS[1:1] structural units elongated in the surface plane. It is expected that the binding interactions of glucose molecule to the BSA:PEDOT-PSS[1:1] solid layer to be different than those with the BSA: PEDOT-PSS[1:1] solute, which changes the glucose detection efficiency for an analyzed fluid sample. In order to detail the glucose binding mechanisms, we studied the surface properties of both Glucose:BSA:PEDOT-PSS[10:1:1]/Ag/Si and Glucose/ BSA:PEDOT-PSS[1:1]/Ag/Si solid layers by AFM, EFM and $F - d$ curves techniques.

3.3. AFM AND EFM RESULTS

The AFM measurements were performed on the exposed surface of Glucose/ Ag/Si, Glucose:BSA:PEDOT-PSS[10:1:1]/Ag/Si and Glucose/BSA:PEDOT-PSS [10:1:1]/Ag/Si deposited by spin-coating and compared with the images from [6]. As it is known, the EFM facility of AFM technique is suitable to characterize the electrical properties of exposed materials surface [11]. The EFM is a double-pass technique, during the first-pass the surface topography is recorded in contact mode with a conductor tip, whereas in the second-pass, the tip rises above the sample surface at the height $\Delta z = 80$ nm and a DC bias voltage (V_{tip}) of 1 V is applied between the tip and sample surface, while the piezo-tube ensures the tip oscillation at its resonance frequency.

In Fig. 4 are represented the topography image (left), surface profile as lateral distance (middle) and electrostatic images as electrostatic potential distribution (right) for all samples. The values of main morphological parameters, as the root mean-square roughness (RMS), arithmetic average roughness (RA), Skewness parameter (SSk), peak-to-valley (Z) determined using a modular software are presented in Table 1.

Taking into account the morphological parameter definitions, the analysis of the above values leads to the following remarks: i) all three layers deposited on the same support have uniform grain structure; the glucose deposited film on the silver film, (a) has lower roughness (0.18 nm) than both the Glucose:BSA:PEDOT-PSS[10:1:1], (b) (0.29 nm) and Glucose/BSA:PEDOT-PSS[1:1], (c) (0.36 nm) layers; ii) more, the Glucose/BSA:PEDOT-PSS[1:1] layer has higher roughness than Glucose: BSA:PEDOT-PSS[10:1:1] and both values are higher than that for the BSA:PEDOT-PSS[1:1] support layer; iii) the profile asymmetry of Glucose/BSA:PEDOT-PSS[1:1] layer (0.63) is much higher than the Glucose:BSA:PEDOT-PSS[10:1:1] (0.079), close to that of BSA:PEDOT-PSS[1:1] support layer (0.04); iv) the Glucose/BSA:PEDOT-PSS[1:1] layer profile height (5.09 nm) is significantly higher than that of Glucose: BSA:PEDOT-PSS[10:1:1] layer (4.58 nm), and both values are higher than that of BSA:PEDOT-PSS[1:1] layer profile (2.17 nm) [6].

Referring to the nanoparticles geometry, we considere that their vertical diameter $d_{vertical}$ may be associated with Z value and the one horizontal $d_{surface}$ (in surface plan) as average value of single peak extension, evaluated from a regulary

repetitive peaks distribution range from the profile curve. Then, axial ratio may be evaluated as $d_{vertical}/d_{surface}$. The evaluated values are listed in Table 1.

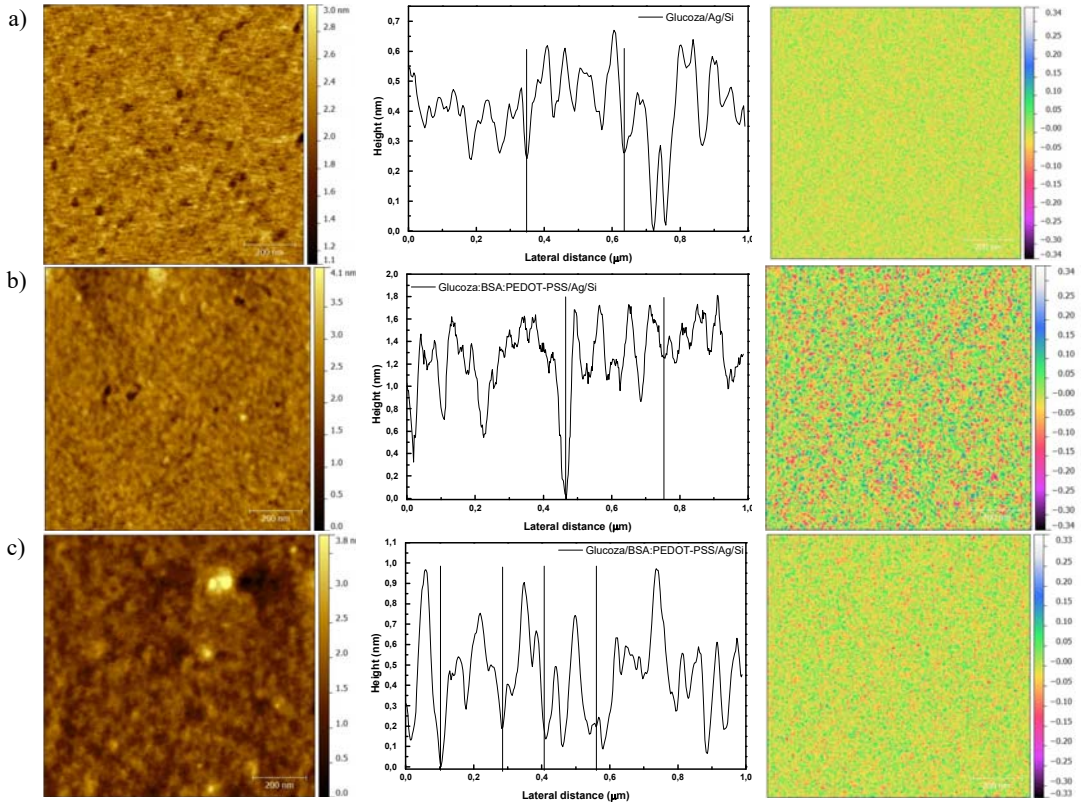

Fig. 4 – AFM records: topography (left), lateral distance (middle) and electrostatic image (right) of a) Glucose/Ag/Si; b) Glucose:BSA:PEDOT-PSS/Ag/Si; c) Glucose/BSA:PEDOT-PSS[1:1]/Ag/Si exposed layers.

Table 1

Values of the morphological and structural parameters of Glucose/Ag/Si, Glucose:BSA:PEDOT-PSS[10:1:1]/Ag/Si and Glucose/BSA:PEDOT-PSS[10:1:1]/Ag/Si layers

Sample	RMS (nm)	RA (nm)	Z (nm)	S_{Skew}	$d_{surface}$ (nm)	Axial ratio
Glucose/Ag/Si	0.18	0.13	3.19	–0.23	70	0.046
Glucose:BSA:PEDOT-PSS/Ag/Si	0.29	0.22	4.58	0.079	70	0.065
Glucose/BSA:PEDOT-PSS/Ag/Si	0.36	0.26	5.09	0.63	150	0.034

The electrostatic images from Fig. 4 (right) show the local potential values generated by the local charge distribution on the explored surface. The areas marked with blue and red correspond to positive and negative charge respectively,

while yellow marks neutral areas. As can be observed, the glucose layer surface (a) has a homogeneous distribution almost neutral, consisting from very small red and blue areas and prevalent yellow areas. Both the Glucose:BSA:PEDOT-PSS[10:1:1] and Glucose/BSA:PEDOT-PSS[1:1] electrostatic images (b) and (c) show that although the homogeneous, potential distribution contains both red and blue of approximately the same surface areas, it is broader than that of the glucose layer. More, the charged surface areas are lower for the Glucose/BSA:PEDOT-PSS[1:1] layer.

3.4. FORCE – DISTANCE RESULTS

The force–distance ($F - z$) curves were performed in the same conditions described in a previous paper [6] on the exposed surface of the solid layer of the Glucose/Ag/Si, Glucose:BSA:PEDOT-PSS[10:1:1]/Ag/Si and Glucose/BSA:PEDOT-PSS[1:1]/Ag/Si structures. The obtained results were compared to the ones obtained on the Ag/Si, BSA/Ag/Si, PEDOT-PSS/Ag/Si, BSA:PEDOT-PSS[1:1]/Ag/Si architectures in order to characterize the properties of the new molecular surface, *i.e.* elasticity, adhesion, density of state [12]. In Figure 5 are illustrated the recorded $F(z)$ curves based on the active layer's surface exploration of the Glucose/Ag/Si (black), Glucose:BSA:PEDOT-PSS[10:1:1]/Ag/Si (red) and Glucose/BSA:PEDOT-PSS[1:1]/Ag/Si (blue) exposed surface.

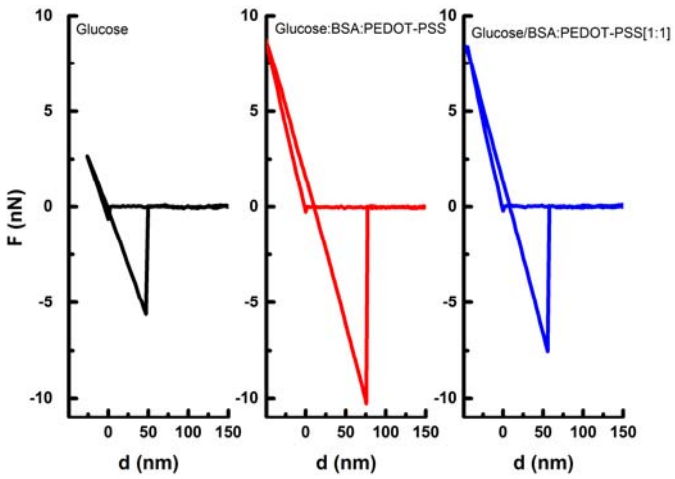

Fig. 5 – $F(z)$ curves recorded on the active layer's surface of: Glucose/Ag/Si (black), Glucose:BSA:PEDOT-PSS[10:1:1]/Ag/Si (red), Glucose/BSA:PEDOT-PSS[1:1]/Ag/Si (blue) structures (Color online).

As in the case of the BSA:PEDOT-PSS[1:1]/Ag/Si layer, by considering the force F [nN] between the semiconducting tip and the layer's surface as elastic,

$F = k \times \Delta d$, we can evaluate the effective elastic constant k of the tip – surface system and subsequently the surface elastic constant [13].

In the snap-off recording mode of $F(z)$, (range between F_{max} and F~0), it is reasonable to consider that the tip-surface circuit is open, and the deformed surface relaxes to equilibrium, so that $F_{max} \approx k_{surface} \times [z\,(F = 0) - d_0\,(F_{max})]$. Thus, the surface elastic constant $k_{surface}$ values were evaluated by averaging values of 20 curves registered on different regions of the explored surface [14]. Both the F_{max} and $k_{surface}$ are listed in Table 2. If we assume that the semiconductor tip-surface interaction is described by the Lennard-Jones 12-6 potential, then by processing the F_{max} and equilibrium distances values extracted from $F(z)$ curves, we can estimate the average surface nanoparticles diameter as $\sigma_{nanoparticle} = 2d_0 - \sigma_{tip}$ (Table 2).

Table 2

The values of main parameters characterizing $F(z)$ measurements and estimated values of surface properties

Sample	F_{max} [nN]	d_o [nm]	$k_{surface}$ [N/m]	$\sigma_{nanoparticle} = 2d_0 - \sigma_{tip}$ [nm]
Glucose/Ag/Si	5.61	47.1	2.31	$2 \times 47.1 - \sigma_{dip}$
Glucose:BSA:PEDOT-PSS[10:1:1]/Ag/Si	10.26	75.8	3.99	$2 \times 75.8 - \sigma_{dip}$
Glucose/BSA:PEDOT-PSS[1:1]/Ag/Si	7.54	55.6	6.22	$2 \times 55.6 - \sigma_{dip}$

4. DISCUSSION

The early performed study results [6] reveal that the BSA:PEDOT-PSS[1:1] protein – polymer mixture acts like a composite in which the protein is included as an integrated part of the new polymeric network, which enables a suitable biocompatible character and a high sensorial efficiency in detecting target biomolecules, through both protein – protein and protein – polymer specific interactions. Thus, the studied composite can be directed towards applications in designing active interface layers to optimize bio detection efficiency through specific interactions between the bioactive exposed surface and the analyzed solvent. When considering the adhesion of the target molecule at biosensor, two main aspects need to be taken into account, *i.e.* molecule shape and surface charge of both partners.

In this study, BSA:PEDOT-PSS[1:1] mixture was used as both active solute and solid active layer deposited by spin-coating, to detect the glucose content in solutions having a large range around biological level. It is known that in the fluids of living organisms, the glucose at normal content in blood (about 1%) plays a vital role in a wide range of biological processes and is considered a basic energy provider, while the glucose excess or deficit may lead to serious health disturbances.

The glucose molecule, as monosaccharide, has two forms, linear open chain and ring of five carbons and oxygen atoms that can polymerize as polysaccharides or oligosaccharides, by binding their ketone or aldehyde terminal functional groups

into great structural diversity. In aqueous solutions, the linear forms coexist with several oligosaccharides. More, in biological fluids, the glucose molecules covalently link to lipids forming glycolipids, with proteins resulting glycoproteins or with other biomolecules and the resulting products properties (current or voltage measured by electrochemistry, fluorescent signal) are both the proof and measure of glucose content. An example of BSA-glucose adhesion reaction is the performance of 380 nM low limit of the CNT/Pt nanosphere biosensor (carbon nanotube and Pt electrodes) regarding the glucose detection [15]. The surface of the CNT electrode functionalized with fluorescently marked BSA exhibits high sensitivity for the enzyme glucose oxidase (GO_x) via covalently linking of BSA with aldehyde terminal groups of glucose molecule. On the other hand, the immobilization efficiency of a solute molecule adhered to the substrate may be analyzed in the Michaelis-Menten equation formalism, which defines the relationship between substrate concentration and solute adhesion rate [16] and appreciated by the effective Michaelis-Menten constant K_M, defined as the substrate concentration at which the solute adhesion rate is half of its saturation value. The K_M may be evaluted processing the transducer signal T_s (electrochemical current, fluorescence signal) with the Lineweaver-Burk double reciprocal plot, $1/T_s = (K_M/T_{sat})(1/c) + (1/T_{sat})$, where T_s and T_{sat} are the steady state and saturation values, respectively. The evolution of the electronic spectra of the Glucose/BSA:PEDOT-PSS[1:1] mixture solution with the glucose concentration (Fig. 1b) demonstrates the binding state of the glucose molecules with the BSA: PEDOT-PSS[1:1] molecules, most likely through mutual interactions favored by their π molecular orbitals overlap. The monochromatic main absorbance value at λ = 278 nm shows a nearly linear dependence of glucose concentration, but with different slopes, of three times higher for high than for low concentrations domains. These concentration ranges are obviously separated by $c = 6.25 \times 10^{-4}$ M that is comparable with the $K_M = 6.4 \times 10^{-4}$ M value evaluated for the CNT/Pt nanosphere biosensor [16], proving that glucose molecules bind to BSA site from BSA:PEDOT-PSS[1:1] structure.

The shape of the dependence from Fig. 1b may be assimilated with the sigmoidal curve (less its saturation) that characterizes the positive cooperative adhesion of a biomolecular ligand on a substrate with affinity for it. Generally, this curve represents the dependence of the fractional occupancy of receptor sites with ligand molecules [17]. The cooperative binding occurs in the case of a substrate with more than one ligand binding site and the binding of a ligand molecule increases the affinity of other ligand molecules to the substrate.

According to Beer-Lambert relationship, $A = \varepsilon dc$, using the same experimental set-up (d is cell length), the slope of the $A = f(c)$ curve expressed by molecular absorbance ε, so that it is reasonable to consider that the up taking glucose molecule is different for low and high glucose content level. Because the monochromatic absorbance shows no shifts and the ATR/FTIR spectrum of mixture solution (Fig. 2) shows the carbonyl C = O, C – C and C – O bond modes of glucose molecules,

we can consider that a glucose content increase induces their polymerization to oligosaccharides. Firstly, at low glucose content level a glucose molecule binds to the BSA:PEDOT-PSS[1:1] substrate *via* BSA affinity sites, and secondly at high glucose level other glucose molecules bind to the already existing glucose molecule that adhered to the substrate. Finally, di- and/or trissacharides are deposited on BSA:PEDOT-PSS[1:1] as substrate.

The results of the structural studies performed using AFM combined with the electrical and elastic properties studies of the bioactive solid layer's surface for Glucose:BSA:PEDOT-PSS[10:1:1] and Glucose/BSA:PEDOT-PSS[1:1] through EFM and $F - z$ techniques highlight particular aspects of the glucose binding on the BSA:PEDOT-PSS[1:1] substrate. In both cases, the nanostructured layer is composed of ellipsoidal nanoparticles with increased sizes as compared with the constituent parts with an in-plane major axis. In addition, in both cases the layer surface contains electrically active insular areas, which are positively and negatively equally charged and uniformly distributed on a continuous neutrally charged background. This distribution can be associated with the existence of both electrically and polar active positions which favors a wide range of interactions with the targeted molecules. Thus, the adhesion interactions of the glucose molecule are electrostatic due to –OH side chain groups and polar due to the dipole moments of aldehyde and ketone terminal groups. Afterwards, binding through C, H, OH free functional groups with other molecules leads to the formation of a structural group of rings, while binding by C, O free terminal functional groups favors open chain structural compounds.

Consequently, both the peak-to valley $Z = 5.09$ nm and in-plain major axis $d_{surface} = 150$ nm of nanoparticles for the Glucose/BSA:PEDOT-PSS[1:1] layer surface are greater than those for BSA:PEDOT-PSS[1:1] support layer, $Z = 2.17$ nm, $d_{surface} = 57$ nm. The consistent polar activity areas ensure a more stable BSA:PEDOT-PSS[1:1] layer in aqueous environments that otherwise may have a corrosive effect *via* electrostatic interactions. Also, the increased elasticity of the solid BSA:PEDOT-PSS[1:1] layer surface favors steric interactions with various target molecules,

It should be noted that all these properties, which enable the increase in bio detection efficiency due to electrically and polar active positions exposure, the nanostructured and electrical nature of the layer, are far superior for the Glucose/ BSA:PEDOT-PSS[1:1] active layer. This result proves the efficiency of the BSA:PEDOT-PSS[1:1] architecture as a bioactive layer.

The quantitative evaluation of the bio detection may be accomplished by means of a transducer signal. Thus, it can be used, for both the solid active layer or composite solution, an optical signal, *i.e.* monochromatic absorbance/fluorescence signal or the electrical current in an electrochemical cell containing the active solution or using the active layers as an electrode. The presence of BSA in the resulting material enables the detection through both the intrinsic fluorescent signal

or through the amplified signal using a suitable labelling of the protein with external fluorophores.

5. CONCLUSIONS

The Glucose:BSA:PEDOT-PSS[10:1:1] mixture was prepared by mixing the glucose solution with the BSA:PEDOT-PSS[1:1] composite solution.

The UV-Vis and ATR/FTIR analysis results on Glucose:BSA:PEDOT-PSS [10:1:1] solution samples highlight a different molecular organization from the constituent parts characterized by an α-helix and β-sheets secondary structure of the BSA, by chains of the PEDOT and by open chains and rings of the glucose. The binding rate of glucose is dependent on its concentration, *i.e.* for concentrations over cca 6×10^{-4}M it nearly doubles.

The as prepared solution was used for the fabrication of a Glucose:BSA: PEDOT-PSS[10:1:1] active solid layer by spin coating deposition on a silver thin film coated silicon substrate. For a comparative study, the other solid layer was fabricated by glucose deposition from solution on a BSA:PEDOT-PSS[1:1] support resulting in a Glucose/BSA:PEDOT-PSS[1:1] architecture.

Their properties where studied using both optical methods, *i.e.* ATR/FTIR and UV-Vis and classical AFM coupled with EFM and $F - z$ technologies. In both cases, the results highlight the formation of a nanostructured composite layer with ellipsoidal nanoparticles with an in-plane major axis and bigger sizes than the constituent parts. The layer has negatively and positively charged exposed insular areas in equal proportions and uniformly distributed in a neutrally charged continuous background. Thus, the layer has both electrically active positions in charged areas and polar active positions in neutral areas, which cover a wide range of interactions with targeted molecules. The deposited layer has superior elastic properties compared to the individual constituent layers, which combined with the ellipsoidal nanostructured components favor steric interactions with various molecules of interest.

It should be noted that all these particularities of the solid composite layer are enhanced in the Glucose/BSA:PEDOT-PSS[1:1] architecture obtained in conditions that mimic those specific to the bio detection procedure consisting of the analysis environment exposure. The polar areas enlargement enables predominantly hydrophobic properties and results in a better stability of the layer in contact with the analyzed environment.

The facile technique and low cost effective fabrication of the studied composites together with the structural properties, biocompatibility and activity of the deposited layers on suitable substrates constitute powerful grounds for their application as interfaces for testing biodevices.

Acknowledgements. The work has been funded by the Sectoral Operational Program Human Resources Development 2007–2013 of the Ministry of European Funds through the Financial Agreement POSDRU/159/1.5/S/137750

REFERENCES

1. Cong Yu, Vivian Wing-Wah Yam, Chem. Commun. **11**, 1347–1349 (2009).
2. Wang J, Chem Rev. **108**, 814–825 (2008).
3. Manju Gerard, Asha Chaubey, B.D. Malhotra, Biosens. Bioelectron. **17**, 345–359 (2002).
4. Adam Heller, Ben Feldman, Chem. Rev. **108**, 2482–2505 (2008)
5. L. Settia, A. Fraleoni-Morgera, B. Ballarin, A. Filippini, D. Frascaro, C. Piana, Biosens. Bioelectron. **20**, 2019–2026 (2005).
6. O. Brîncoveanu, A. Ioanid, S. Iftimie, J. Al-Zanganawee, M. Enachescu, S. Antohe, Dig. J. Nanomater. Biostruct. **11**, 833–843 (2016).
7. Yuya Egawa, Ryota Gotoha, Toshinobu Sekib, Jun-ichi Anzaia, Mater. Sci. Eng.: C **1**, 115–118 (2009)
8. L.Z. Wu, B.L. Ma, D.W. Zou, Z.X. Tie, J. Wang, W. Wang., J. Mol. Struct. 8**77**, 44–49 (2008).
9. Jintian Liang, Wentian Zeng, Pingjia Yao, Yuanan Wei, Adv. Bio. Chem. **2**, 226 –232(2012).
10. Marie-Astrid Ottenhof, William MacNaughtan, Imad A. Farhat, Carbohydr. Res. **338**, 2195–2202 (2003).
11. E. Mikamo-Satoh, F. Yamada, A. Takagi, T. Matsumoto, T. Kawai, Nanotech. **20**, 145102 (2009)
12. Hans-Jurgen Butt, Brunero Cappella, Michael Kappl, Surf. Sci. Rep. **59**, 1–152 (2005)
13. Chun-Chih Lai, Nunzio Motta and John M. Bell, Int. J. Nanosci. **7**, 299–303 (2008).
14. Devendra Khatiwada, Shobha Kanta Lamichhane, The Himalayan Phy. **2**, 80–83 (2011).
15. J.C. Claussen, S.S. Kimm, A. Haque, M.S. Artiles, D.M. Porterfield, T.S. Fisher, J. Diabetes Sci. Technol. **4**, 312–319 (2010).
16. Nelson, David L. and Michael M. Cox. Lehninger, *Principles of Biochemistry*. 5th Edition, NY. W.H. Freeman and Company, New York, 2008.
17. Sanders, Charles R, *Biomolecular Ligand-Receptor Binding Studies: Theory, Practice, and Analysis*, Vanderbilt University 1–42, 2010.